Indian Journal of Pure & Applied Physics
Vol. 63, December 2025, pp. 1132-1146
DOI: 10.56042/ijpap.v63i12.21857

Numerical Investigation of Efficient Active Flow Control Around the Airfoil NACA 0015 With Plasma DBD Actuators

Abdelhakim Amine Djendara[a*], Sadek Gouasmi[b] & Mohamed Amine Khiari[b]

[a]Department of mechanical engineering, University of Science and Technology, Oran 310 00, Algeria
[b]Department of mechanical engineering, National Polytechnic School, Oran 310 00, Algeria

Received :21st July 2025; accepted:23rd September 2025

There are considerable studies to optimize the lift coefficient with the plasma Multi Dielectric Barrier Discharge (MDBD) actuators over the airfoil profiles, either in terms of location or in terms of the number of actuators used. All of these studies focused only on the upper side of the airfoils, ignoring the lower one, which can also undergo significant change on one hand, and on the other hand, the majority of studies don't take control efficiencies into consideration. For this reason, this study performs tests on both sides (upper and lower surfaces) by changing the location and the number of activated actuators on the airfoil profile, where the first step is to ensure the optimal configuration on the upper surface and then test the lower surface by means of two control configurations: "With" (which induces flow velocity) and "Inverse" (which reduces flow velocity), by installing five actuators on the upper surface and five others on the lower surface of the NACA0015 airfoil profile of 150 mm chord length, where the latter are disposed symmetrically to the upper ones placed uniformly at chordal locations x/c = (0.1, 0.3, 0.5, 0.7, 0.9). The actuators are activated by means of 7 kV in "steady state" (100% duty cycle), with a flow Reynolds number Re ≈ 35000, representative of low-to-moderate Reynolds aerodynamic applications such as UAVs and wind-tunnel conditions. The ANSYS Fluent program is adapted for this process, in collaboration with a user-defined function (UDF) compiled with the integrated electric potential module to carry out the computation. The results show promising values in lift and efficiency, especially by identifying three relevant flight modes compared to the baseline mode. The first is the Max Lift Mode, which is detected at 15° and reaches an extreme lift coefficient with a notable lift force gain; the second mode reaches its best values at 10°, also with a maximum lift gain force, where it is remarkable that the actuator near the trailing edge with "Inverse" configuration contributes to improving the result; and finally, the High Efficiency Mode is also detected at 10°, with maximum efficiency and lift coefficient, and a net lift force gain.

Keywords: MDBD, Active control, Lift coefficient, Lift efficiency, Power consumption, Plasma actuator

1. Introduction

The control of boundary layer separation has long been recognized as a key challenge in aerodynamics, as it directly affects lift, drag, and overall efficiency. Among the various approaches, active flow control has gained significant attention due to its adaptability and absence of moving mechanical parts, making it highly reliable and responsive[1]. Within active methods, dielectric barrier discharge (DBD) plasma actuators are of particular interest because of their fast response, low power consumption, and silent operation without electrode erosion[2].

Extensive experimental research has examined the performance of DBD actuators under different conditions. Studies have highlighted the influence of applied voltage[3], operating frequency and waveform[4], actuator geometry[5], dielectric material selection[6], and placement strategy[7]. Collectively, these efforts underline the sensitivity of actuator performance to both electrical and geometric parameters.

In parallel, numerical models have been developed to better capture the underlying plasma–flow interactions. Hydrodynamic models have described actuator flow coupling[8], while subsequent improvements incorporated ion dynamics[9] and chemical reactions[10]. Further refinements addressed pressure dependence for in-flight applications[11], photoionization effects[12], and simplified representations for practical simulations[13,14].

Despite these advances, the use of multiple actuators has shown limitations in efficiency due to increased power demand without proportional aerodynamic benefits[15]. This motivates the present investigation, which evaluates plasma actuation on both upper and lower surfaces of a NACA 0015 airfoil. The approach employs the Spalart–Allmaras turbulence model[16] within ANSYS Fluent[17],

*Corresponding author: E-mail: djendara3188@gmail.com

integrating potential field calculations and charge density distributions based on Gaussian boundary conditions[18]. By systematically varying actuator placement and number, over 800 cases are analyzed to identify configurations that maximize lift while minimizing energy consumption. The proposed methodology is supported experimentally by[19].

2 Computational scheme

2.1 Governing Equations

To evaluate the effect of body force produced by actuators, this work examines more than 800 test cases covering various actuator configurations. A simplified plasma model is applied for that, by computing the electric field via the potential module in Fluent and the charge density from a Laplace equation. Their product provides the induced body force, added to the momentum equation as a UDF like a source term:

2.1.1 Plasma Body Force Equations

To determine the plasma body force, the steps of computation are as follows:

2.1.1.1 Potential Equation

The spread of the electric potential in both fluid and dielectric domain is described by:

$$\nabla.(\varepsilon\nabla\Phi) = 0 \quad \text{... (1)}$$

The symbol ε denotes the medium permittivity, which in air is assumed to be equal to the vacuum permittivity :($\varepsilon_0 = 8.854 \times 10^{-12}\mathrm{Fm}^{-1}$);while in the dielectric layer $\varepsilon_d = 5\varepsilon_0$; and Φis the electric field in the medium with the unit[V] or [$\mathrm{kg.s}^{-3}\mathrm{A}^{-1}$].

2.1.1.2 Electric Field

After solving the potential using Eq. (1), the corresponding electric field applied to the fluid and dielectric zones is computed from the expression

$$\vec{E} = -\Delta\Phi \quad \dots 2$$

2.1.1.3 Electric Density

Tocompute the generated electric volume density, we use also the Laplace equation since it is very simple and faster inspiring from Orlov[13], Suzan & Huang[20] models.

$$\nabla.\left(\varepsilon_0\nabla\rho\right) = 0 \quad \dots 3$$

The neglected source term is here accounted for by incorporating it into the boundary condition, which allows proper calibration.

2.1.1.4 Electric Body Force

Multiplying the electric density from Eq. (3) with the electric field from Eq. (2) provides the body force at each computation cell, which is required as a source term in the momentum equation.

$$\vec{F}_b = \rho.\vec{E} \quad \dots 4$$

And from this stage, it becomes straightforward to calculate the total induced body force required to evaluate the airfoil efficiency:

$$F_{b,total} = \sum \rho_{Air}.E.Vcell \quad \dots 5$$

ρ_{Air} :Is fluid density, Vcell : is the cell volume.

2.1.2 Gas Dynamics Equations

2.1.2.2 Continuity Equation

The continuity equation guarantees mass conservation by imposing a divergence-free condition on the velocity field in incompressible flow, thereby ensuring constant fluid density and eliminating any net mass accumulation within the computational domain.

$$\frac{\partial u_i}{\partial x_i} = 0 \quad \dots 6$$

2.1.2.3. Momentum Equation

The momentum equation expresses Newton's second law applied to a fluid element**,** describing how the rate of change of momentum is governed by the balance between inertial, pressure, viscous, and added plasma body forces. By incorporates the effects of turbulence and flow unsteadiness, providing a fundamental framework for analyzing fluid motion, aerodynamic loads, and energy transfer mechanisms within the flow field.

$$\rho\left(\frac{\partial u_i}{\partial t} + u_i\frac{\partial u_i}{\partial x_i}\right) = -\frac{\partial p}{\partial x_i} + \frac{\partial}{\partial x_j}\left[(\mu+\mu_t) + \left(\frac{\partial u_i}{\partial x_j} + \frac{\partial u_j}{\partial x_i}\right)\right] + \rho f_i + F_{b,i} \quad \dots 7$$

u_i : Mean velocity; ρ: density; p : mean pressure.
μ: Molecular dynamic viscosity.
μ_t : Turbulent (eddy) dynamic viscosity (given by SA below).
f_i : Other body forces (gravity, etc.).
$F_{b,i}$: Plasma induced body force per unit volume.

This latter we introduce it through a user-defined function (UDF).

2.1.2.4 Turbulence Equation

For modeling the gas dynamics, a mass-averaged approach was applied to describe the motion of the

gas throughout the fluid domain over the airfoil. In this framework, the incompressible RANS Spalart-Allmaras formulation is considered as follows:

$$\frac{\partial}{\partial t}\left(\rho\tilde{v}\right)+\frac{\partial}{\partial x_i}\left(\rho\tilde{v}u_i\right)=G_v+\frac{1}{\sigma_{\tilde{v}}}\left[\frac{1}{\partial x_j}\left\{\left(\mu+\rho\tilde{v}\right)\frac{\partial\tilde{v}}{\partial x_j}\right\}+C_{b2}\rho\left(\frac{\partial\tilde{v}}{\partial x_j}\right)^2\right]-Y_v+S_{\tilde{v}} \quad \ldots 8$$

Where $\tilde{v}$ denotes the turbulent kinematic viscosity except in the near-wall region. G_v and Y_v represent, respectively, the production and destruction terms of turbulent viscosity, both mainly active in the near-wall zone. The coefficients $\sigma\tilde{v}$ and C_{b2} are model constants. All parameters of the Spalart–Allmaras formulation applied in this work retain Fluent's default values[17], except for the Courant number, set to 250, which improves numerical stability and accelerates steady convergence, The term $S\tilde{v}$ denotes the turbulence source term, implemented through a user-defined function (UDF).

2.1.3 Airfoil Profile Efficiency

Since the interaction of the plasma actuator is implemented as an explicit source term inside the momentum equation using UDF text which is interpreted with ANSYS Fluent, the computed aerodynamic forceis:

$$F_{lift}=S_{profile}.\rho_{air}.Cl.u^2 \quad \ldots 9$$

$S_{profile}$: is the chordale surface of the airfoil profile. Cl : is the lift coefficient of the airfoil and u is the free streamvelocity.

And by using Eq.(5) we have the following equations:

$$\eta_{lift}=\frac{\Delta F_{lift}}{F_{b,total}} \quad \ldots 10$$

where:

$$\Delta F_{lift}=F_{lift,total}-F_{lift,baseline} \quad \ldots 11$$

$F_{lift,baseline}$: The lift force obtained without control.

$F_{lift,total}$: The lift force obtained with control.

3 Test Case Configuration

3.1 Computational Domain

The computational domain is a C-type grid extending 20 chord lengths in the normal direction and 25 chord lengths downstream of the trailing edge toward the outlet. These dimensions were chosen to minimize boundary effects and to ensure accurate resolution of the flow field and wake structures around the airfoil, as recommended in similar plasma-based flow control studies[21]. The configuration of these test cases is illustrated in Fig. 1.

3.2 Mesh Formulation

The fluid domain was discretized using a structured mesh of approximately 25 × 600 computational cells[22], including 100 layers in the wall-normal direction and 500 cells distributed along the airfoil cross-section. The first cell height was set to $e = 5.10^{-3}$ mm, corresponding to $Y+\in[5,30]$, which ensures an adequate near-wall resolution and

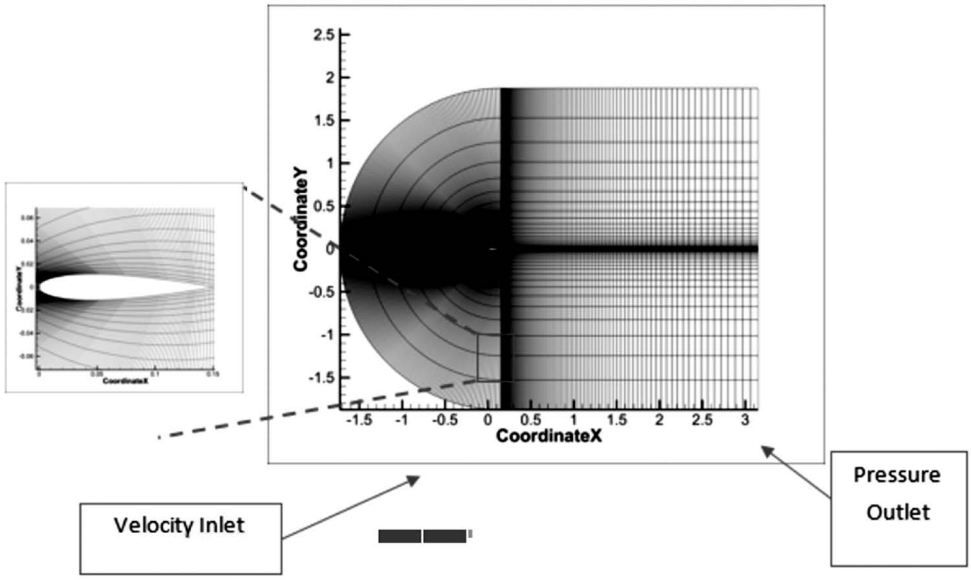

Fig. 1 — Demonstration of the fluid computational domains

yields lift coefficient values Cl in good agreement with available experimental data[15]. For the dielectric region, a single cell layer was employed across the thickness of 130 μm**,** while 10 transverse cells were introduced per electrode which assure the stability and reliability and in order to accurately capture the local electric field distribution and ensure proper coupling with the plasma actuator.

3.3 Computational Program

The simulation was performed using the density-based solver with second-order upwind discretization of the 2D finite volume method. The coupled algorithm was applied for the flow equations to improve stability and convergence, while the plasma model was computed separately in another Fluent session using the SIMPLE algorithm, which is more efficient for solving electrostatic potential fields. The plasma results were exported as CSV files and imported as user-defined scalars (UDS) to be introduced as source terms in the flow solution.

3.4 Actuator Geometry

The electrode dimensions were taken from[15], with both the exposed and covered electrodes having a width of 7 mm and a length of 150 mm. The dielectric layer beneath the electrodes had a thickness of 130 μm. The actuators were uniformly distributed along the chord at positions x/c= (0.1, 0.3, 0.5, 0.7, 0.9) on both the upper and lower surfaces of the airfoil.

3.5 Boundary Conditions

3.5.1 Fluid Model

The working fluid was incompressible air, modeled as steady-state, with a free-stream velocity of $\bar{u}$ = 3.8 m/s[15], corresponding to a Reynolds number of $Re \approx 35{,}000$. This velocity was imposed at all inlet boundaries, as illustrated in Fig. 1. A pressure outlet condition was applied at the domain exit, while the airfoil surface and actuator walls were treated as no-slip boundaries.

3.5.2 Plasma Model

The plasma boundary conditions consist of two parts. The first corresponds to the potential module, where the applied voltage is set to $\Phi_{App} = 7000$ V at the anode of an activated actuator and $\Phi = 0$ V at the cathode, while for deactivated actuators and elsewhere a zero-flux condition $\frac{\partial \Phi}{\partial n} = 0$ is imposed. For the electric charge density, a Gaussian distribution is prescribed as:

$$\rho_{App} = \rho_{max} e^{\left(\frac{-(x-\mu)^2}{2\sigma^2}\right)} \quad \ldots 12$$

It is necessary to calibrate $\rho_{max} = 0.00153\ C/m^3$ to reach the value of 50% of lift growth which it means an error $\approx 0\%$ by using the actuators $x/c = 0.1$[15],while it set to be$\rho_{App} = 0$ for deactivated actuators and the rests of boundaries the used Gaussian coefficients in this case is $\sigma = \mu = 1$. And x is the location.

Meanwhile we distinct two configurations of plasma boundaries condition Fig. 2:

3.5.2.1 Normal Configuration:

The standard orientation in that induce the flow which the cathode and anode are arranged conventionally, applied to all sides of airfoil.

3.5.2.2 Inversed Configuration:

Identical to the normal case, except that the electrode polarity is reversed on the lower surface, i.e., the electrodes are interchanged. This configuration can decelerate the local fluid flow[23].

4 Results

The first stage of the computation consists of extracting the lift coefficients and their corresponding efficiency for angles of attack of 0°, 5°, 10°, 15°, and 20°, using 320 Fluent test cases with the aforementioned boundary configurations. After processing, the results are presented in the graphs below. Figure 3 (a) shows the effect of actuator activation by number, where the configuration (UL5+DLI5) gives the maximum value. In comparison, Fig. 3 (b) demonstrates that a single actuator located appropriately provides a value comparable to that obtained in Fig. 3 (a) These findings highlight the influence of activation strategy.

The local actuator efficiency by the following term:

$$\eta_{Local} = 0{,}5\rho U_{\infty}{}^2 Cl / F_{electric} \quad \ldots 13$$

And the corresponding values are reported in Table 1. The total efficiency control system is defined by:

$$\eta_{Total} = 0{,}5\rho U_{\infty}{}^2 Cl / F_{electric} = \eta_{Local} \quad \ldots 14$$

The maximum values in Tables 1 and 2 are $\eta_{Local} = \eta_{Total} = 2.64$ with $Cl = 0.27$. And by contrast, the peak lift coefficient of $Cl = 0.37$ corresponds to the lower total efficiency: $\eta_{Total} = 1.82$.

The net lift gain is determined as follows:

$$\Delta F_{Net} = F_{lift,total} - F_{lift,baseline} - F_{electric} \quad \ldots 15$$

While the Table 3 shows that several actuator configurations achieve $\eta_{Total} > 1$ with the best case yielding of $\Delta F_{Net} = 0{,}22$ N correspond to Cl = 0,27.

At the A.O. A=5°, we applied the same aforementioned process. Figure 4 (a) illustrates the variation of lift coefficient with the number of activated actuators, where the configuration (ALL+DNI5) provides the peak value. Where the graph shows that this configuration outperforms the other tested cases. In turn, Fig. 4 (b) presents the variation of lift coefficient with actuator location, where it is observed that the configuration (ALL+DLI5) achieves superior Case of activation (ALL+DLI5**)** gives a best results.

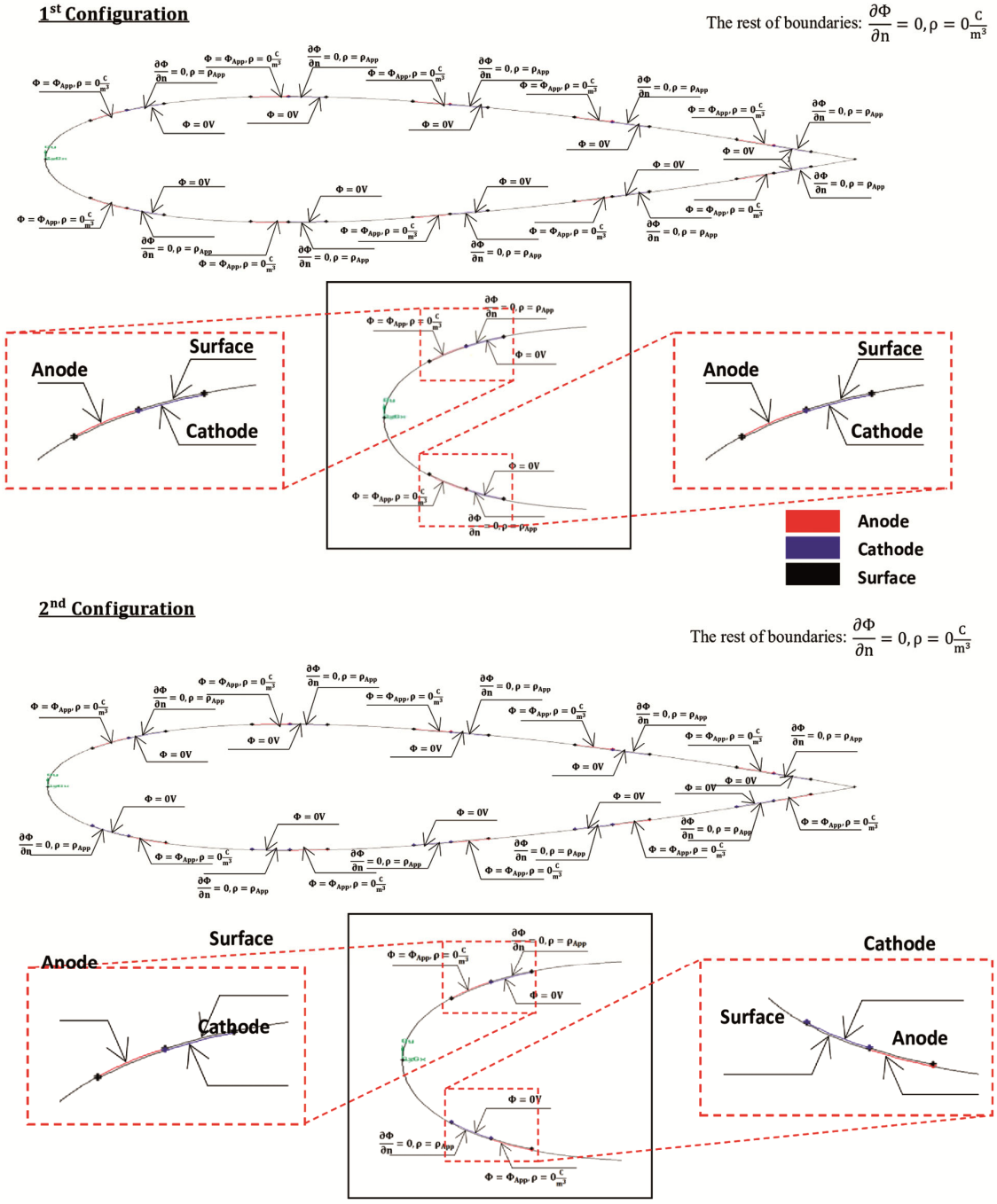

Fig. 2 — Illustrations of the electric boundary conditions actuators “With” and “inverse” configurations

Results compared with the case in Fig. 4 (a), reaching a coefficient of lift $Cl = 0{,}91$.This outcome is further justified by the efficiencies reported in Tables 4 and 5, where the maximum value of efficiency $\eta_{Total} = 2{,}57$ is consistently obtained.

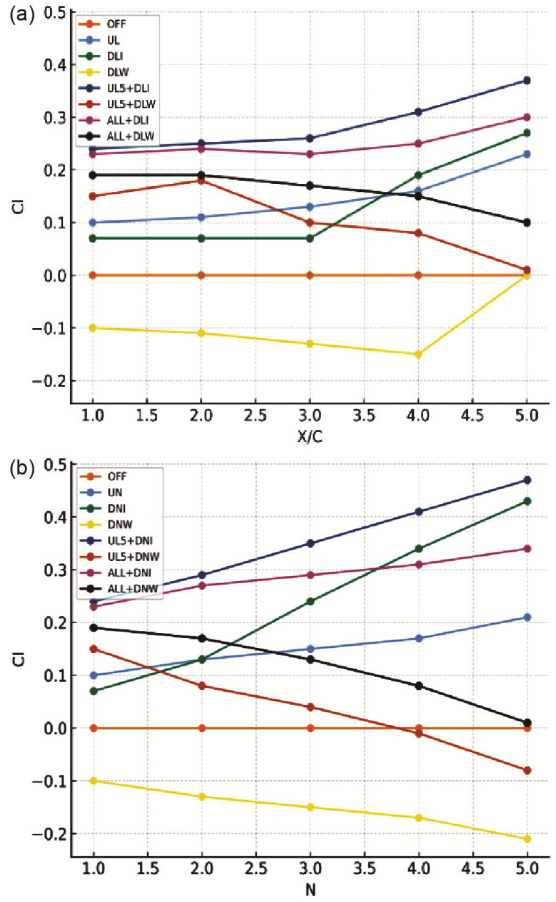

Fig. 3 — Lift Coefficient (a) by location(b) by number for angle of 0°

However, the Table 6 highlights a different results, showing that the highest net lift gain of $\Delta F_{net} = 0{,}31N$ corresponds to the configuration (UL5+DLI5), with a lift coefficient of $Cl = 0.86$.

The first stage of the computation consists to extract the lift coefficient and their lift efficiency for the subsequent angle of attack of $0{,}5{,}10{,}15{,}20°$ by mean of 137 tests of the tree aforementioned test The first

At the angle of 10°, the same steps described previously were applied. Fig. 5 (a) illustrates the variation of lift coefficient with the number of activated actuators, showing that the configuration (ALL+DNI5) provides the peak value with $Cl = 1.37$. In turn, Fig. 5 (b) presents the variation of lift coefficient with actuator location, where it is clearly observed that the configuration (ALL+DLI5) achieves the maximum value $Cl = 1.39$ with only 6 actuators

To justify these results, the local and total efficiencies reported in the Tables 7 and 8 indicate that $\eta_{Local} = \eta_{Total} = 3{,}15$, which is the highest value obtained for the configuration (UL3+DLI5) with $Cl = 0{,}84$. Meanwhile, theTable 9 provides further insight, showing that the peak of net lift force gain with the value $\Delta F_{Net} = 0{,}35N$ which it corresponds to the control configuration (ALL+DLI5) with a $Cl = 1{,}39$.

At the angle of 15°, the same procedure applied for the previous cases was followed. Figure 6-a shows the variation of lift coefficient with the number of activated actuators, where the configuration (ALL+DNW5) produces the peak value with $Cl = 1.03$. In turn, Fig. 6 (b) illustrates the variation of lift coefficient with actuator location, showing that the

Table 1 — The variations of the obtained local actuator lift efficiency at angle of 0° the orange in the maximum (DLI5)

ACT X/C	UN	UL	DNW	DLW	DNI	DLI	UL5+ DNW	UL5+ DLW	UL5+ DNI	UL5+ DLI	ALL+ DNW	ALL+ DLW	ALL+ DNI	ALL+ DLI
1	1,01	1,01	-1,03	-1,03	0,64	0,64	-0,78	-0,78	0,13	0,13	-0,19	-0,19	0,14	0,14
2	0,32	1,11	-0,32	-1,13	0,62	0,70	-0,64	-1,27	0,49	0,26	-0,46	-0,26	0,55	0,30
3	0,20	1,32	-0,20	-1,35	1,16	0,68	-0,46	-1,24	0,60	0,29	-0,84	-0,38	0,79	0,19
4	0,14	1,54	-0,13	-1,53	0,96	1,90	-0,48	-1,51	0,56	0,86	-1,33	-0,58	0,95	0,41
5	0,44	2,25	-0,41	0,00	0,86	2,64	-0,71	-2,13	0,63	1,39	-2,04	-1,12	1,31	0,87

Table 2 — The variations of the obtained total airfoil lift efficiency at angle of 0° the orange in the maximum (DLI5)

ACT X/C	UN	UL	DNW	DLW	DNI	DLI	UL5+ DNW	UL5+ DLW	UL5+ DNI	UL5+ DLI	ALL+ DNW	ALL+ DLW	ALL+ DNI	ALL+ DLI
1	1,01	1,01	-1,03	-1,03	0,64	0,64	0,73	0,73	1,19	1,19	0,15	0,15	0,37	0,37
2	0,66	1,11	-0,68	-1,13	0,63	0,70	0,27	0,49	0,96	1,25	0,07	0,12	0,38	0,40
3	0,51	1,32	-0,52	-1,35	0,81	0,68	0,09	0,51	0,87	1,27	-0,01	0,07	0,36	0,38
4	0,41	1,54	-0,42	-1,53	0,84	1,90	-0,02	0,37	0,80	1,55	-0,09	0,00	0,34	0,42
5	0,42	2,25	-0,42	0,00	0,85	2,64	-0,14	0,06	0,78	1,82	-0,22	-0,21	0,34	0,49

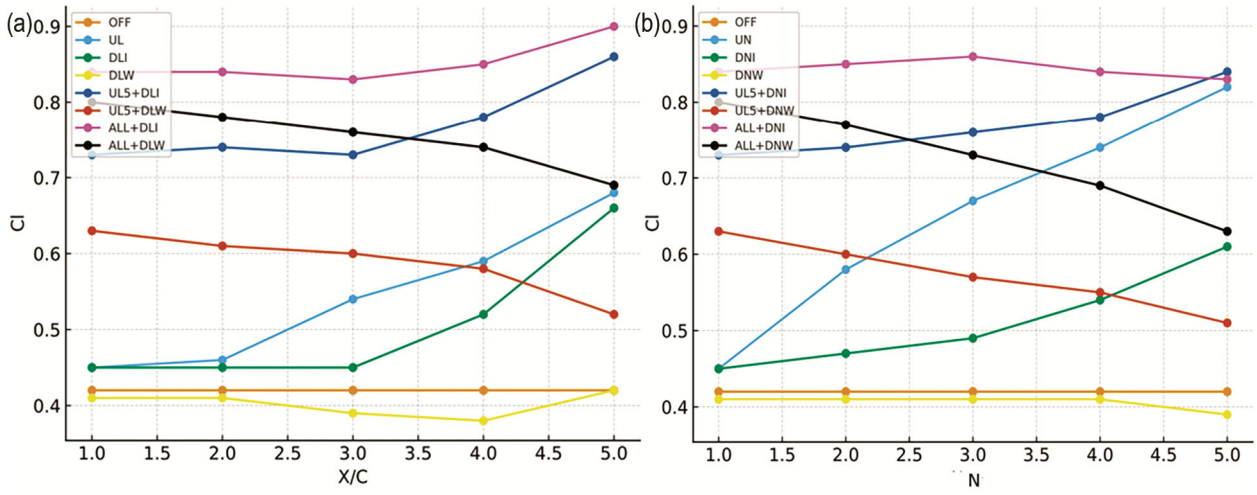

Fig. 4 — Lift Coefficient (a) by location (b) by number for angle of 5°

Table 3 — The variations of the net lift force gain ΔF_{net}[N] at angle of 0°the orange is the maximum (UL5+DNI5)

ACT X/C	UN	UL	DNW	DLW	DNI	DLI	UL5+ DNW	UL5+ DLW	UL5+ DNI	UL5+ DLI	ALL+ DNW	ALL+ DLW	ALL+ DNI	ALL+ DLI
1	0,13	0,13	-0,14	-0,14	0,09	0,09	0,20	0,20	0,32	0,32	0,25	0,25	0,30	0,30
2	0,18	0,15	-0,18	-0,15	0,17	0,09	0,11	0,13	0,38	0,33	0,22	0,24	0,35	0,32
3	0,20	0,18	-0,21	-0,18	0,32	0,09	0,05	0,13	0,46	0,34	0,17	0,23	0,38	0,30
4	0,22	0,21	-0,22	-0,20	0,45	0,25	-0,02	0,10	0,54	0,41	0,10	0,20	0,41	0,33
5	0,28	0,30	-0,28	0,00	0,56	0,35	-0,11	0,02	0,62	0,48	0,01	0,13	0,45	0,40

Table 4 — The variations of the obtained local actuator lift efficiency at angle of 5°the colored is the maximum (UL5)

ACT X/C	UN	UL	DNW	DLW	DNI	DLI	UL5+ DNW	UL5+ DLW	UL5+ DNI	UL5+ DLI	ALL+ DNW	ALL+ DLW	ALL+ DNI	ALL+ DLI
1	0,24	0,24	-0,13	-0,13	0,22	0,22	-0,55	-0,55	0,50	0,50	-0,23	-0,23	0,22	0,22
2	1,27	0,40	-0,01	-0,17	0,18	0,27	-0,28	-0,68	0,09	0,56	-0,52	-0,38	0,31	0,20
3	0,93	1,15	-0,02	-0,32	0,26	0,27	-0,27	-0,87	0,22	0,45	-0,91	-0,58	0,38	0,10
4	0,66	1,67	0,06	-0,45	0,48	0,98	-0,24	-1,06	0,14	0,97	-1,27	-0,78	0,21	0,27
5	0,81	2,57	-0,25	0,00	0,71	2,30	-0,43	-1,65	0,66	1,73	-1,87	-1,32	0,16	0,86

Table 5 — The variations of the obtained total airfoil lift efficiency at angle of 5° the colored is the maximum (UL5)

ACT X/C	UN	UL	DNW	DLW	DNI	DLI	UL5+ DNW	UL5+ DLW	UL5+ DNI	UL5+ DLI	ALL+ DNW	ALL+ DLW	ALL+ DNI	ALL+ DLI
1	0,24	0,24	-0,13	-0,13	0,22	0,22	1,01	1,01	1,54	1,54	0,61	0,61	0,69	0,69
2	0,75	0,40	-0,07	-0,17	0,20	0,27	0,58	0,94	1,05	1,56	0,48	0,59	0,60	0,69
3	0,81	1,15	-0,06	-0,32	0,22	0,27	0,37	0,85	0,85	1,51	0,38	0,55	0,54	0,67
4	0,78	1,67	-0,03	-0,45	0,28	0,98	0,25	0,75	0,70	1,77	0,29	0,52	0,46	0,70
5	0,78	2,57	-0,07	0,00	0,37	2,30	0,13	0,46	0,70	2,15	0,20	0,43	0,41	0,80

control type (UL3+DLI5) achieves a value of Cl = 0.92 with only six actuators, comparing with Ten in the configuration (ALL+DNW5) in Fig. 6(a).

To justify these results, the efficiencies reported in Table 10 shows that the highest local efficiency of $\eta_{Local} = 1{,}09$ is obtained by the configuration (UN2), while their corresponding total efficiency Sin Table 11 is reduced to $\eta_{Total} = 0{,}90$. It is therefore evident that $\eta_{Total} < 1$, which indicating that the flight under this condition is energetically unfavorable. Furthermore; The Table 12 confirms this trend, showing that the greatest net force value is negative, with $\Delta F_{Net} = -0{,}02N$ at the configuration (UL2).

Eventually atthe angle A. O. A=20 the same procedure was performed. Figure 7 (a) displays the variation of lift coefficient with the number of activated actuators, where the configuration (ALL+DNW5) provides the peak value with

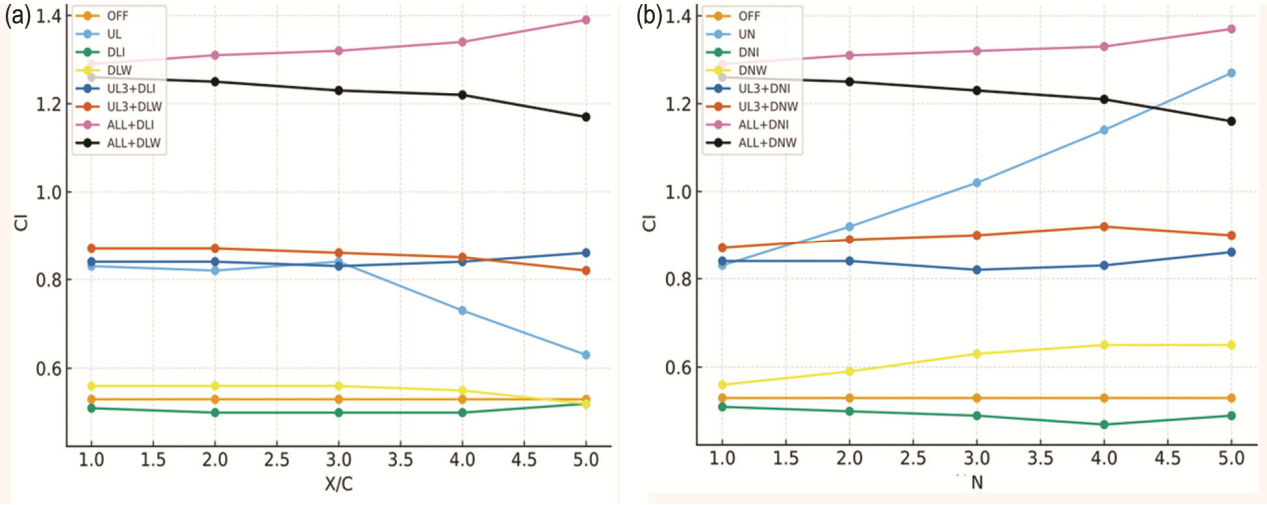

Fig. 5 — Lift Coefficient (a) by location (b) by number for angle of 10°

Table 6 — The variations of the net lift force gain ΔF_{net}[N] at angle of 5° the colored is the maximum (UL5+DLI5)

ACT X/C	UN	UL	DNW	DLW	DNI	DLI	UL5+ DNW	UL5+ DLW	UL5+ DNI	UL5+ DLI	ALL+ DNW	ALL+ DLW	ALL+ DNI	ALL+ DLI
1	0,03	0,03	-0,02	-0,02	0,03	0,03	0,27	0,27	0,41	0,41	0,49	0,49	0,55	0,55
2	0,20	0,05	-0,02	-0,02	0,05	0,04	0,23	0,25	0,42	0,42	0,45	0,47	0,56	0,55
3	0,33	0,15	-0,02	-0,04	0,09	0,04	0,20	0,23	0,45	0,40	0,40	0,44	0,57	0,53
4	0,41	0,22	-0,01	-0,06	0,15	0,13	0,16	0,20	0,47	0,47	0,35	0,42	0,55	0,56
5	0,52	0,34	-0,05	0,00	0,25	0,31	0,11	0,12	0,56	0,57	0,27	0,35	0,54	0,64

Table 7 — The variations of the obtained local actuator lift efficiency at angle of 10° the colored cell is the maximum (UL3)

ACT X/C	UN	UL	DNW	DLW	DNI	DLI	UL3+ DNW	UL3+ DLW	UL3+ DNI	UL3+ DLI	ALL+ DNW	ALL+ DLW	ALL+ DNI	ALL+ DLI
1	2,98	2,98	0,35	0,35	-0,12	-0,12	0,25	0,25	0,00	0,00	-0,09	-0,09	0,20	0,20
2	0,95	2,93	0,33	0,36	-0,13	-0,24	0,18	0,23	-0,06	-0,05	-0,22	-0,24	0,35	0,36
3	0,93	3,15	0,33	0,32	-0,12	-0,26	0,18	0,15	-0,15	-0,14	-0,42	-0,39	0,44	0,42
4	1,24	2,06	0,27	0,23	-0,15	-0,24	0,16	0,06	0,05	-0,05	-0,65	-0,55	0,53	0,62
5	1,32	1,08	-0,03	-0,05	0,15	-0,07	-0,17	-0,27	0,29	0,20	-1,13	-1,07	0,99	1,18

Table 8 — The variations of the obtained total airfoil lift efficiency at angle of 10° the colored cell is the maximum (UL3)

ACT X/C	UN	UL	DNW	DLW	DNI	DLI	UL3+ DNW	UL3+ DLW	UL3+ DNI	UL3+ DLI	ALL+ DNW	ALL+ DLW	ALL+ DNI	ALL+ DLI
1	2,98	2,98	0,35	0,35	-0,12	-0,12	1,70	1,70	1,58	1,58	0,73	0,73	1,27	1,27
2	1,97	2,93	0,34	0,36	-0,13	-0,24	1,19	1,69	1,03	1,55	0,61	0,71	1,11	1,30
3	1,62	3,15	0,33	0,32	-0,13	-0,26	0,94	1,65	0,74	1,51	0,48	0,65	0,98	1,31
4	1,53	2,06	0,32	0,23	-0,13	-0,24	0,79	1,60	0,60	1,55	0,53	0,80	0,89	1,34
5	1,49	1,08	0,25	-0,05	-0,07	-0,07	0,63	1,44	0,55	1,67	0,52	0,88	0,84	1,44

Table 9 — The variations of the net lift force gain ΔF_{net}[N] at angle of 10° the colored cell is the maximum (ALL+DLI5)

ACT X/C	UN	UL	DNW	DLW	DNI	DLI	UL3+ DNW	UL3+ DLW	UL3+ DNI	UL3+ DLI	ALL+ DNW	ALL+ DLW	ALL+ DNI	ALL+ DLI
1	0,26	0,26	-0,09	-0,09	-0,15	-0,15	0,19	0,19	0,15	0,15	0,18	0,18	0,22	0,22
2	0,26	0,26	-0,18	-0,09	-0,30	-0,16	0,08	0,18	0,01	0,15	0,03	0,16	0,10	0,24
3	0,25	0,29	-0,27	-0,09	-0,45	-0,17	-0,03	0,17	-0,14	0,14	-0,13	0,14	-0,02	0,25
4	0,28	0,14	-0,36	-0,10	-0,60	-0,17	-0,14	0,16	-0,27	0,15	-0,30	0,12	-0,14	0,27
5	0,32	0,01	-0,50	-0,14	-0,72	-0,14	-0,30	0,12	-0,36	0,18	-0,49	0,05	-0,21	0,35

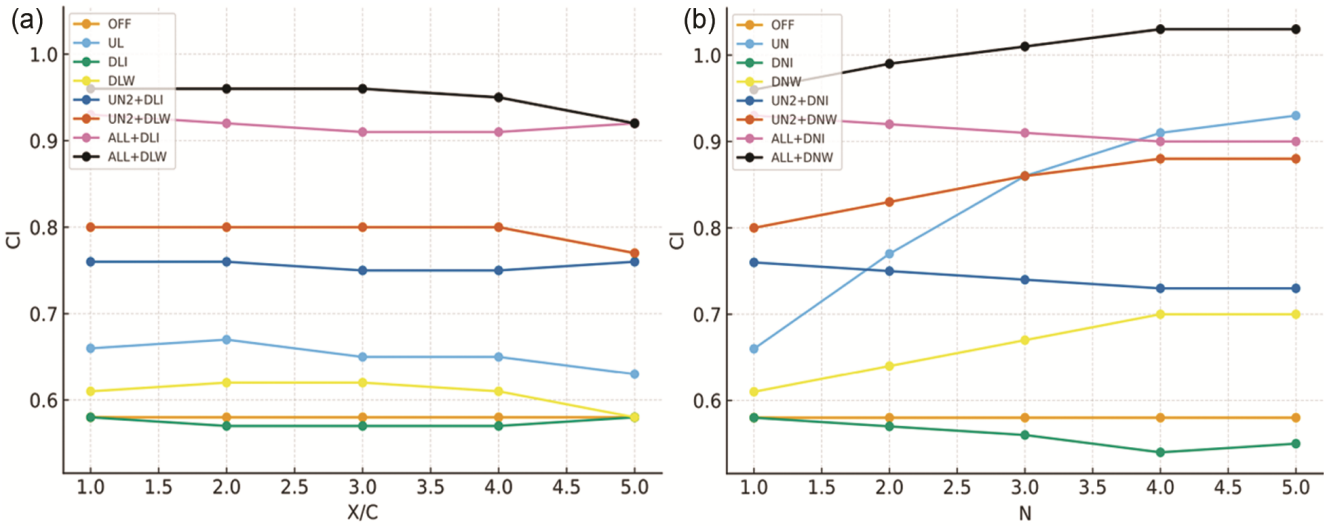

Fig. 6 — Lift Coefficient (a) by location(b) by number for angle of 15°

Table 10 — The variations of the obtained local actuator lift efficiency at angle of 15° the colored cell is the maximum (UN2)

ACT X/C	UN	UL	DNW	DLW	DNI	DLI	UN2+ DNW	UN2+ DLW	UN2+ DNI	UN2+ DLI	ALL+ DNW	ALL+ DLW	ALL+ DNI	ALL+ DLI
1	0,72	0,72	0,29	0,29	-0,06	-0,06	0,33	0,33	-0,03	-0,03	0,35	0,35	0,03	0,03
2	1,09	0,84	0,30	0,34	-0,09	-0,17	0,28	0,36	-0,09	-0,10	0,61	0,34	-0,03	-0,08
3	0,89	0,66	0,30	0,33	-0,12	-0,18	0,29	0,30	-0,11	-0,14	0,84	0,32	-0,15	-0,13
4	0,50	0,66	0,28	0,24	-0,14	-0,18	0,22	0,30	-0,13	-0,14	1,01	0,22	-0,26	-0,13
5	0,21	0,48	-0,04	-0,02	0,07	-0,04	-0,04	0,04	0,02	-0,05	1,01	-0,02	-0,26	-0,06

Table 11 — The variations of the obtained total airfoil lift efficiency at angle of 15° the colored cell is the maximum (UN2)

ACT X/C	UN	UL	DNW	DLW	DNI	DLI	UN2+ DNW	UN2+ DLW	UN2+ DNI	UN2+ DLI	ALL+ DNW	ALL+ DLW	ALL+ DNI	ALL+ DLI
1	0,72	0,72	0,29	0,29	-0,06	-0,06	0,71	0,71	0,59	0,59	0,51	0,51	0,57	0,57
2	0,90	0,84	0,29	0,34	-0,07	-0,17	0,61	0,72	0,42	0,57	0,45	0,49	0,48	0,55
3	0,90	0,66	0,30	0,33	-0,09	-0,18	0,54	0,70	0,03	0,56	0,45	0,51	0,41	0,55
4	0,80	0,66	0,29	0,24	-0,10	-0,18	0,49	0,70	0,24	0,56	0,42	0,49	0,35	0,55
5	0,68	0,48	0,23	-0,02	-0,07	-0,04	0,41	0,62	0,21	0,58	0,39	0,48	0,31	0,56

Table 12 — The variations of the net lift force gain ΔF_{net}[N] at angle of 15° the colored cell is the maximum (UL2)

ACT X/C	UN	UL	DNW	DLW	DNI	DLI	UN2+ DNW	UN2+ DLW	UN2+ DNI	UN2+ DLI	ALL+ DNW	ALL+ DLW	ALL+ DNI	ALL+ DLI
1	-0,04	-0,04	-0,09	-0,09	-0,14	-0,14	-0,11	-0,11	-0,16	-0,16	-0,30	-0,30	-0,34	-0,34
2	-0,03	-0,02	-0,19	-0,09	-0,29	-0,16	-0,21	-0,11	-0,31	-0,17	-0,40	-0,30	-0,48	-0,36
3	-0,04	-0,05	-0,28	-0,09	-0,44	-0,16	-0,31	-0,12	-6,86	-0,18	-0,50	-0,30	-0,63	-0,36
4	-0,11	-0,05	-0,38	-0,10	-0,59	-0,16	-0,41	-0,12	-0,61	-0,18	-0,61	-0,32	-0,78	-0,36
5	-0,21	-0,07	-0,52	-0,14	-0,71	-0,14	-0,55	-0,15	-0,74	-0,17	-0,74	-0,35	-0,91	-0,35

$Cl = 0.99$. While in Fig. 7 (b) shows the variation of lift coefficient with actuator location, and it is remarkable that the configuration (ALL+DLW1) achieves a comparable result to that in Fig. 7 (a), with $Cl = 0.92$ using only six actuators instead of ten.

To examine these results, the efficiencies presented in Tables 13 and 14 are considered. It is observed that the maximum efficiency value of $\eta_{Total} = 0.73$ is obtained in both cases, but since $\eta_{Total} < 1$, the configuration is not energetically favorable. In addition, Table 15 confirms this conclusion, as the greatest net lift force value is negative, with $\Delta F_{net} = -0{,}04N$. These outcomes indicate that at 20° the flight condition becomes inefficient, and the control

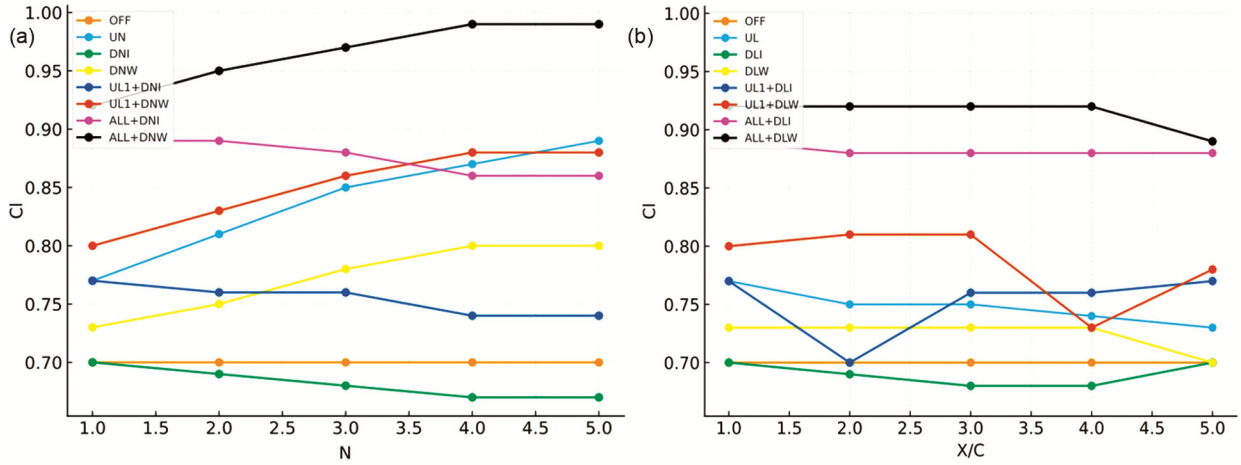

Fig. 7 — Lift Coefficient (a) by location (b) by number for angle of 20°

Table 13 − The variations of the obtained local actuator lift efficiency at angle of 20° the colored cell is the maximum (UN1)

ACT X/C	UN	UL	DNW	DLW	DNI	DLI	UL1+ DNW	UL1+ DLW	UL1+ DNI	UL1+ DLI	ALL+ DNW	ALL+ DLW	ALL+ DNI	ALL+ DLI
1	0,73	0,73	0,26	0,26	-0,06	-0,06	0,26	0,25	-0,02	-0,02	0,30	0,30	0,01	0,01
2	0,37	0,47	0,28	0,32	-0,07	-0,14	0,27	0,33	-0,07	-0,73	0,56	0,34	-0,05	-0,09
3	0,35	0,47	0,28	0,33	-0,09	-0,16	0,28	0,35	-0,09	-0,16	0,79	0,33	-0,14	-0,14
4	0,26	0,42	0,21	0,24	-0,10	-0,16	0,20	-0,49	-0,12	-0,17	0,96	0,24	-0,26	-0,14
5	0,19	0,33	-0,02	0,00	0,03	-0,04	-0,01	0,03	0,00	-0,06	0,98	0,00	-0,29	-0,08

Table 14 — The variations of the obtained total airfoil lift efficiency at angle of 20°the colored cell is the maximum (UN1)

ACT X/C	UN	UL	DNW	DLW	DNI	DLI	UL1+ DNW	UL1+ DLW	UL1+ DNI	UL1+ DLI	ALL+ DNW	ALL+ DLW	ALL+ DNI	ALL+ DLI
1	0,73	0,73	0,26	0,26	-0,06	-0,06	0,49	0,49	0,35	0,35	0,36	0,36	0,32	0,32
2	0,55	0,47	0,27	0,32	-0,06	-0,14	0,42	0,53	0,21	0,00	0,35	0,37	0,26	0,30
3	0,48	0,47	0,27	0,33	-0,07	-0,16	0,38	0,54	0,14	0,28	0,33	0,37	0,22	0,29
4	0,43	0,42	0,26	0,24	-0,08	-0,16	0,35	0,12	0,09	0,28	0,32	0,35	0,18	0,29
5	0,38	0,33	0,20	0,00	-0,06	-0,04	0,29	0,38	0,07	0,33	0,29	0,31	0,16	0,30

Table 15 — The variations of the net lift force gain ΔF_{net}[N] at angle of 20° the colored cell is the maximum (UN1)

ACT X/C	UN	UL	DNW	DLW	DNI	DLI	UL1+ DNW	UL1+ DLW	UL1+ DNI	UL1+ DLI	ALL+ DNW	ALL+ DLW	ALL+ DNI	ALL+ DLI
1	-0,04	-0,04	-0,10	-0,10	-0,14	-0,14	-0,14	-0,14	-0,17	-0,17	-0,51	-0,51	-0,55	-0,55
2	-0,12	-0,07	-0,20	-0,09	-0,28	-0,15	-0,23	-0,13	-0,32	-0,27	-0,61	-0,50	-0,69	-0,56
3	-0,21	-0,07	-0,29	-0,09	-0,43	-0,16	-0,33	-0,12	-0,46	-0,19	-0,71	-0,50	-0,83	-0,57
4	-0,31	-0,08	-0,40	-0,10	-0,58	-0,15	-0,43	-0,23	-0,61	-0,19	-0,82	-0,52	-0,98	-0,57
5	-0,42	-0,09	-0,53	-0,13	-0,70	-0,14	-0,57	-0,17	-0,74	-0,18	-0,95	-0,55	-1,12	-0,56

strategy cannot provide a useful aerodynamic advantage.

The second stage of this computation consists to compute the lift coefficients and their efficiencies for the subsequent angles of attack of (0°,5°,10°,15°,20°) by mean of 100 tests of the following controlling types (ALL, UL5, DLI5, UL5 + DLI5, ALL + DLI5), since it gives interesting results compared to the rest controlling types, and this by changing the force scale (F/F0) from (1 to 5) by 1.

Where the Fig. 8 shows the variation of liftfor the first angle we can see that the types (DLI5), (UL5+DLI5) provide a important values with a reached peak by activating only one actuator in (DLI5), with $Cl = 0{,}86$ and force scale $F/F0 = 5$.

To investigate this value, we introduce the Table 16 which illustrates their related total efficiencies, and we find that the obtained result (lift coefficient peak) is $\eta_{total} = 1{,}70$.

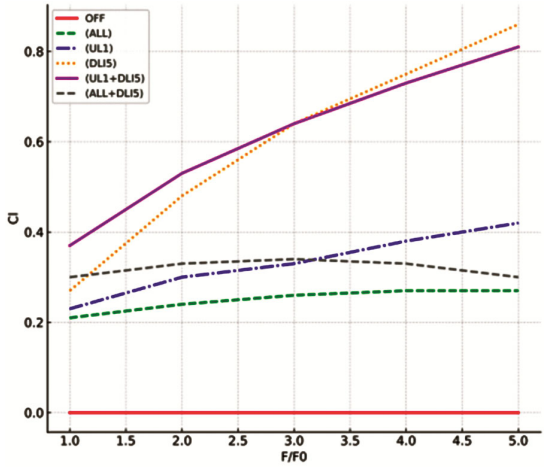

Fig. 8 — Lift Coefficient by force augmentation of 0°

Table 16 — Total efficiency by multiplying F/F0 at 0°

F/F0	ALL	UL5	DLI5	UL5+ DLI5	ALL+ DLI5
1	0,42	2,25	2,64	1,82	0,49
2	1,12	4,90	4,96	3,16	1,04
3	0,17	1,10	2,10	1,06	0,19
4	0,13	0,93	1,85	0,91	0,13
5	0,11	0,83	1,70	0,81	0,10

Table 17 — Net force gain by multiplying F/F0 at 0°

F/F0	ALL	UL5	DL5I	UL5+ DLI5	ALL+ DLI5
1	-0,39	0,17	0,22	0,22	-0,40
2	-1,02	0,12	0,37	0,16	-1,17
3	-1,66	0,04	0,44	0,05	-1,96
4	-2,32	-0,03	0,45	-0,10	-2,77
5	-2,98	-0,11	0,47	-0,26	-3,61

While the peak value of the total efficiency at this angle is obtained by controlling type (DLI5) at $F/F0 = 2$ of $\eta_{total} = 4{,}96$, which corresponds to a value of only $Cl = 0{,}48$.

Table 17 shows the net gain; we can see that the best is the same obtained in high lift coefficient with the type (DLI5), $F/F0 = 5$ with $\Delta F_{net} = 0{,}47N$.

Figure 9 shows the variation of lift for the second angle (A.O.A=5°) with the same controlling configurations, and it is remarkable that the controlling type (UL5+DLI5) provides the highest results for nearly all F/F0, with a peak $Cl = 1{,}38$, and secondly the type (DLI5) with $Cl = 1{,}34$, while the control (ALL+DLI5) reaches its peak at $F/F0 = 2$ and then decreases

Therefore, the control by (UL5) ranks in third place but remains far from the other best classified controlling types.

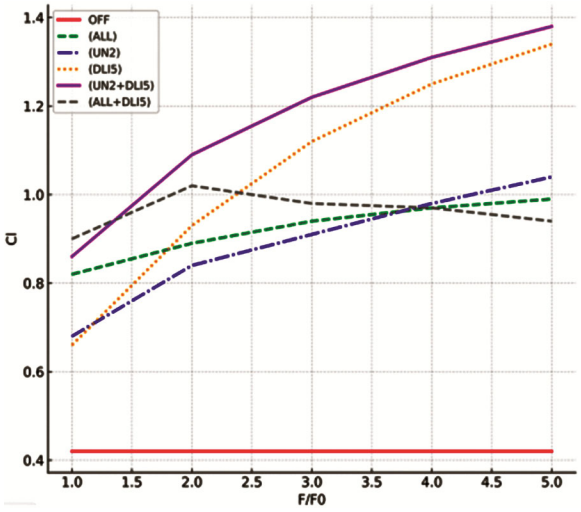

Fig. 9 — Lift Coefficient by force augmentation of 5°

Table 18 — Local efficiency by multiplying F/F0 at 5°

F/F0	ALL	UL5	DLI5	UL5+ DLI5	ALL+ DLI5
1	0,78	2,57	2,30	2,15	0,80
2	0,46	2,06	2,51	1,66	0,50
3	0,34	1,62	2,31	1,32	0,30
4	0,27	1,38	2,06	1,10	0,23
5	0,23	1,22	1,82	0,95	0,17

Table 19 — Net force gain [N] by multiplying F/F0 at 5°

F/F0	ALL	UL5	DL5I	UL5+ DLI5	ALL+ DLI5
1	-0,15	0,21	0,17	0,31	-0,16
2	-0,72	0,28	0,40	0,35	-0,81
3	-1,32	0,25	0,53	0,25	-1,67
4	-1,94	0,20	0,56	0,10	-2,48
5	-2,58	0,15	0,54	-0,07	-3,32

To analyse these values, the Table 18 illustrates their efficiencies, we find that the value of the obtained maximum lift coefficient gives $\eta_{total} = 0{,}37$, while the best value of the total efficiency is obtained by the control type (UL5) at $F/F0 = 1$ with $\eta_{total} = 2{,}57$, corresponding to $Cl = 0{,}68$,

This indicates that not always the maximum Cl gives the appropriate control but the effect is rather defined by the best compromise between lift and efficiency.

Table 19 shows the net gain, it is evident that the best is the same obtained in the high lift coefficient by the control (DLI5), $F/F0 = 4$ with $\Delta F_{net} = 0{,}56N$.

In the A.O.A=10° we study the selected control types (ALL,UL3,DLI5,UL3+DLI5,ALL+DLI5) , since they present the most significant values, and by the Fig. 10 it is observable that the controlling type

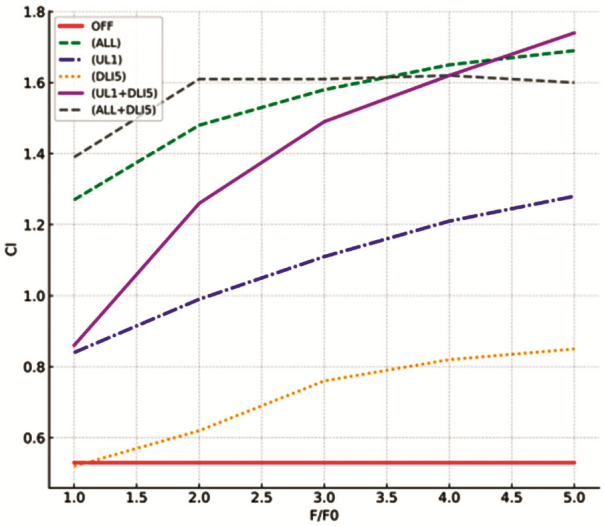

Fig. 10 — Lift Coefficient by force augmentation at 10 °

Table 20 — Total efficiency by multiplying F/F0 at 10 °

F/F0	ALL	UL3	DLI5	UL3+ DLI5	ALL+ DLI5
1	1,49	3,15	-0,07	1,67	1,44
2	0,95	2,33	0,47	1,82	0,90
3	0,70	1,95	0,77	1,60	0,60
4	0,56	1,69	0,72	1,36	0,45
5	0,46	1,50	0,65	1,21	0,36

Table 21 — Net force gain [N] by multiplying F/F0 10 °

F/F0	ALL	UL3	DLI5	UL3+ DLI5	ALL+ DLI5
1	0,32	0,29	-0,14	0,18	0,35
2	-0,07	0,35	-0,14	0,44	-0,16
3	-0,60	0,38	-0,09	0,48	-0,96
4	-1,18	0,37	-0,15	0,38	-1,75
5	-1,79	0,33	-0,24	0,28	-2,58

(UL3+DLI5) provides the highest value with $\mathrm{Cl} = 1{,}74$ at the range of $\mathrm{F/F0} = 5$, and secondly the control type (ALL) with $\mathrm{Cl} = 1{,}69$, followed by the control (ALL+DLI5), while the controls (UL3) and (DLI5) give lower values, which reveals that the use of one actuator alone is not sufficient for the control at this angle.

To verify the obtained results, we introduce directly Table 20 which illustrates the correspondent total efficiencies of the lift coefficients, where the value of the maximum lift coefficient gives $\eta_{total} = 1{,}21$, so it is clear that the flight with this value is close to the minimum ($\eta_{total} = 1$).

While the best efficiency value is obtained in the controlling type (UL3) at $\mathrm{F/F0} = 1$with $\eta_{total} = 3{,}15$, corresponding to $\mathrm{Cl} = 0{,}84$. To choose the acceptable maximum lift coefficient, Table 21

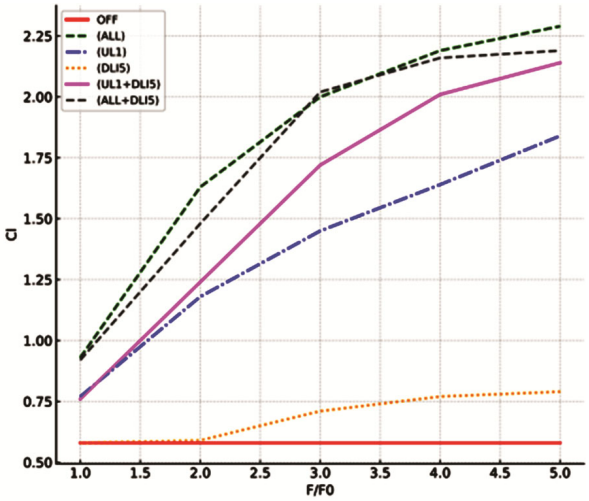

Fig. 11 — Lift Coefficient by force augmentation at 15 °

Table 22 — Total efficiency by multiplying F/F0 at 15 °

F/F0	ALL	UN2	DLI5	UN2+ DLI5	ALL+ DLI5
1	0,68	0,90	-0,04	0,58	0,56
2	1,04	1,48	0,01	1,08	0,75
3	0,94	1,44	0,41	1,26	0,79
4	0,80	1,31	0,47	1,19	0,65
5	0,68	1,25	0,42	1,03	0,53

indicates the net lift force gain, where we can see that the best obtained value appears for the control type (UL3+DLI5), $\mathrm{F/F0} = 3$, with $\Delta F_{net} = 0{,}48\mathrm{N}$, which corresponds to a lift coefficient $\mathrm{Cl} = 1{,}49$.

And then for the angle of attack A.O.A=15° we verify the selected flow control types via (ALL,UN2,DLI5,UN2+DLI5,ALL+DLI5), which are the best control types at this angle, where after Fig. 11 it is clear that the controlling type (ALL) and then (ALL+DLI5) provide approximately the highest results for all ranges of F/F0, with the peak value obtained at $\mathrm{F/F0} = 5$ by the (ALL) control type with $\mathrm{Cl} = 2{,}29$. We can also see that the type (UN2+DLI5) at F/F0=5 gives an interesting value with $\mathrm{Cl} = 2{,}14$ by using only three actuators.

To understand the behavior of these values, we refer to the total efficiencies in Table 22, which illustrates these results, where the corresponding value of the maximum lift coefficient gives $\eta_{total} = 0{,}68$, so it is inconvenient to fly with this value even if Cl is maximum since the efficiency $\eta_{total} < 1$.

Meanwhile, the best total efficiency is obtained in (UN2) at F/F0=2 by $\eta_{total} = 1{,}48$, at $\mathrm{Cl} = 1{,}18$, which is near the efficiency peak, and after this value this later begins to decrease. It is not able that even

Table 23 — Net force gain [N] by multiplying F/F0 15 °

F/F0	ALL	UN2	DLI5	UN2+ DLI5	ALL+ DLI5
1	-0,21	-0,03	-0,14	-0,17	-0,35
2	0,06	0,26	-0,26	0,07	-0,40
3	-0,13	0,35	-0,24	0,31	-0,50
4	-0,54	0,33	-0,28	0,30	-1,12
5	-1,07	0,33	-0,39	0,07	-1,87

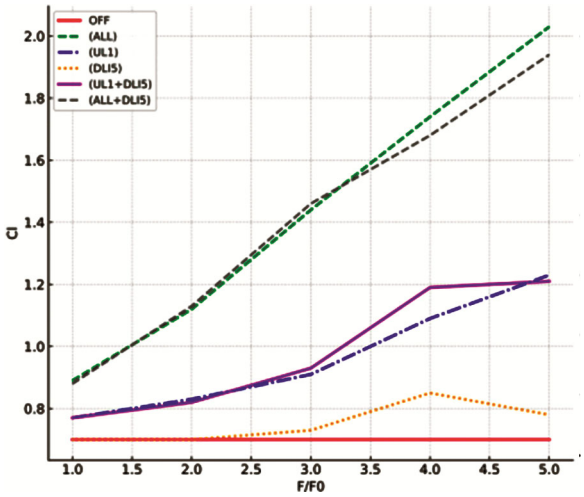

Fig. 12 — Lift Coefficient with the force augmentation 20 °

with the decrease of efficiency the value remains $\eta_{total} > 1$, which reveals an additional lift force gain. Table 23 indicates that the peak is by the control (UN2), F/F0=3 with $\Delta F_{net} = 0{,}47N$ and $Cl = 1{,}45$.

Eventually, by studying the flow control at the angle of attack A.O.A=20° with the best selected control types (ALL,UL1,DLI5,UL1+DLI5,ALL+ DLI5), we obtain the lift coefficients by force augmentation in Fig. 12, and it is apparent that the control type (ALL) provides the peak value at $F/F0 = 5$ with $Cl = 2{,}03$, followed by the control type (ALL+DLI5), while the other controlling types remain with small values, especially in the case of using one actuator only, where the activation of actuator number has a remarkable effect at this angle.

By investigating the related total efficiencies depicted in Table 24, the first remark is that for all control types with several activated actuators, the total efficiency remains inferior to one, showing that the control is not convenient with these values, and the second remark is that there is an increase of efficiency in the control type (UL1) by augmentation of the force scale F/F0 until the maximum value $F/F0 = 5$, where it reaches $\eta_{total} = 1{,}05$, corresponding to $Cl = 1{,}23$.

Table 24 — Total efficiency by multiplying F/F0of 20°

F/F0	(ALL)	(UL1)	(DLI5)	(UL1+ DLI5)	(ALL+ DLI5)
1	0,38	0,73	0,67	0,33	0,30
2	0,42	0,63	-0,02	0,15	0,36
3	0,49	0,71	0,11	0,19	0,42
4	0,52	0,97	0,37	0,12	0,41
5	0,53	1,05	0,16	0,11	0,41

Table 25 — Net force gain by multiplying F/F0 20 °

F/F0	(ALL)	(UL1)	(DLI5)	(UL1+ DLI5)	(ALL+ DLI5)
1	-0,42	-0,04	-0,04	-0,18	-0,56
2	-0,77	-0,10	-0,27	-0,91	-1,03
3	-1,01	-0,12	-0,36	-1,30	-1,40
4	-1,29	-0,02	-0,34	-1,48	-1,90
5	-1,57	0,03	-0,56	-1,99	-2,36

Table 26 — Additional best results of force on the actuator*

F/F0	Cl(10°) (UL2+ DL5I)	η(10°) (UL2+ DL5I)	Δf(10°) (UL2+ DL5I)	Cl(15°) (UL2)	η(15°) (UL2)	Δf(15°) (UL2)
1	0,84	1,56	0,42	0,67	0,84	0,11
2	1,66	2,83	1,51	0,80	1,09	0,29
3	1,55	1,70	1,36	1,04	1,51	0,60
4	1,67	1,42	1,51	1,24	1,63	0,87
5	1,76	1,23	1,64	1,38	1,58	1,05

Table 25 explores the next verification by computing the net force gain, where we can see that all forces with any control type give negative values except (UL1) at $F/F0 = 5$, which provides $\Delta F_{net} = 0{,}03N$ with $Cl = 1{,}23$.

Finally it is convenient is to investigate the effect of force multiplication on the adjacent best actuators and we introduce in the Table 26 directly where the best obtained results are observed in (10°,15°), that give a peak values obtained in (UL2+DLI5) for 10° at $F/F0 = 3$ and (UL2) in 15 ° when $F/F0 = 3$.

xBy studying the angles (2.5°,7.5°,12.5°,17.5°) in same way like first angles we earn the Fig. 13 which compare the selected best values of each parameter, we observe that there are 4 flights modes the first is Max lift mode but $\eta_{Total} < 1$ then saturation mode $\eta_{Total} \approx 1$ and high efficiency and high net lift gain modes with $\eta_{Total} > 1$.

By ignoring the max lift mode since $\eta_{Total} < 1$ we will have the Table 27 that explore the efficiencies and gains of the 2 left convenient flight modes:

After all that analyses it is possible to conclude that the A.O.A 10° get a max efficiency and net lift force gain that let us investigate behavior of their flow.

Figure 14 shows the effect of velocities and flow pattern and it is observable that in the upper surface the flow is attached in both (b) & (c) comparing to (a) while in lower surface we observe the effect of (DLI5) on (c) which reducing the flow velocity and generate little turbulence which create convenient additional force but this let us inquire about the drag coefficient since it decelerates the flow, the Table 28 comparedrag coefficient of the three cases.

Through the results of this Table, we can conclude that the is no augmentation of the drag coefficient in the third case due to the fluid flow reduction comparing to the obtained addition force gain.

Table 27 — Total efficiency by multiplying the Fb of 20°*

Flight mode	High Efficiency mode		High gain lift ΔF_{net} mode	
A.O.A	η_{Total}	ΔF_{net}[N]	η_{Total}	ΔF_{net}[N]
0°	4,96	0,37	1,70	0,47
2,5°	2,73	0,36	1,95	0,51
5°	2,57	0,21	2,06	0,56
7,5°	2,33	0,18	2,13	0,45
10°	3,15	0,29	2,83	0,97
12,5°	2,34	0,36	1,72	0,76
15°	1,63	0,34	1,58	0,39
17,5°	1,26	1,17	1,26	1,17
20°	1,05	0,03	1,05	0,03

Table 28 — Drag coefficient for the three selected cases

Mode of Control	Drag Coefficient
Base line	0,11
Highest efficiency	0,07
Up + down	0,07

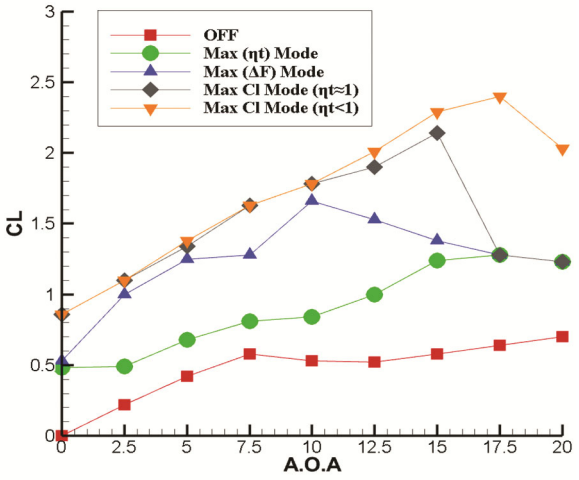

Fig. 13 — The selected better value for each angle

5 Appendix

Table 29 — Drag coefficient for the three selected cases

Abbreviations	Signification
UN	Up by number
UL	Up by location
DLW	Down by location (with)
DNW	Down by number (with)
DLI	Down by location (inverse)
DNI	Down by number (inverse)
BU+DLW	Best up + Down by location (with)
BU+DNW	Best up + Down by number (with)
BU+DLI	Best up + Down by location (inverse)
BU+DNI	Best up + Down by number (inverse)
ALL+DLW	All activated + Down by location (with)
ALL+DNW	ALL + Down by number (with)
ALL+DLI	ALL + Down by location (inverse)
ALL+DNI	ALL + Down by number (inverse)
N^{th}	The activated actuator number

Table 30 — The flow control types of the selected convenient flight modes in obtained in the Table 27

A.O.A	High η_{Total}	F/F0	High gain lift ΔF_{net} mode	F/F0
0°	(DL5I)	2	(DLI5)	5
2,5°	(DL5I)	1	(DLI5)	4
5°	(UL5)	1	(DLI5)	4
7,5°	(UL5)	1	(DLI5)	3
10°	(UL3)	1	(UL2+DLI5)	2
12,5°	(UL1)	2	(UN2+DLI5)	4
15°	(UL2)	4	(UL2)	5
17,5°	(UL1)	5	(UL1)	5
20°	(UL1)	5	(UL1)	5

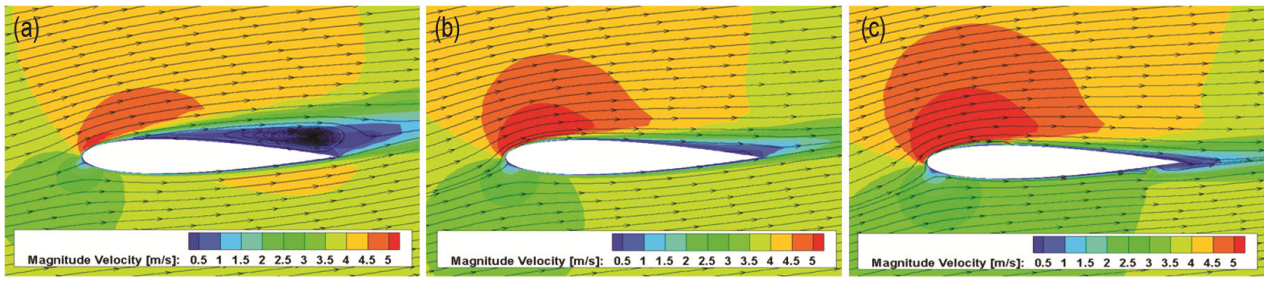

Fig. 14 — Velocity contours of the selected modes of controls (a) baseline, (b) highest efficiency, (c) highest gain lift force

6 Conclusion

This work has presented a detailed numerical analysis of active flow control on NACA0015 airfoil using ten plasma DBD actuators. The investigation was carried out in two main stages: the first examined different actuator configurations on both the upper and lower surfaces, while the second assessed the effect of multiplying the generated body forces up to five times, resulting in over 800 test cases. The combined results lead to several meaningful conclusions. On the upper surface, activating only one actuator proved sufficient to obtain optimal performance, highlighting the efficiency of localized control. On the lower surface, the placement of a single actuator near the trailing edge produced an additional lift contribution. From the overall evaluation, three relevant flight modes were identified: the high efficiency mode, the maximum net lift gain mode, and the high lift (saturation) mode. The first two modes reached their best results at an A.O.A of 10°, while the last was found most effective at 15°. Importantly, the configurations that altered the bottom near trailing edge achieved significant lift improvements with negligible drag increase, confirming the promising potential of plasma-based actuation for efficient aerodynamic performance.

References

1 Gad-El-Hak M, *Flow Control: Passive, Active, and Reactive Flow Management*, Cambridge: Cambridge University Press, 2000.

2 Corke T C & Post M L, Overview of plasma flow control: Concepts, optimization, and applications, *AIAA Paper*, (2005) 563, https://doi.org/10.2514/6.2005-563.

3 Thomas F O, Corke T C, Iqbal M, Kozlov A & Schatzman D, *AIAA J*, 47 (9) (2009) 2169, https://doi.org/10.2514/1.41788.

4 Benard N & Moreau E, *Exp Fluids*, 55 (11) (2014) 1846.

5 Jayaraman B & Shyy W, *Prog Aerosp Sci*, 44 (3) (2008) 139.

6 Tang A, *et al*, *J Phys D Appl Phys*, 56 (35) (2023) 355201.

7 Lagmich Y, Callegari T, Pitchford L C, Boeuf J P, *J Phys D Appl Phys*, 41 (9) (2008) 095205.

8 Shang J S & Huang P G, *Prog Aerosp Sci*, 67 (2014) 29.

9 Abdollahzadeh M, Pascoa J C & Oliveira P J, *Comput Fluids*, 128 (2016) 77.

10 Jayaraman B, 38th *AIAA plasmadynamics and laser conference*, (2007) 4531, https://doi.org/10.2514/6.2007-4531.

11 Kriegseis J, Simon B & Grundmann S, *J Phys D Appl Phys,* 49 (5) (2016) 054006.

12 Likhanskii A, Semak V & Opaits D, The role of photoionization in numerical modeling of the DBD actuator, *AIAA Paper*, (2009) 841, https://doi.org/10.2514/6.2009-841.

13 Orlov D M, *Modeling and Simulation of Single Dielectric Barrier Discharge Plasma Actuators*, Notre Dame (IN): University of Notre Dame, 2006.

14 Li X, Xu J & Zhang Y, *Aerosp Sci Technol*, 118 (2021) 107030.

15 Akansu Y E, Karakaya F & Şanlısoy A, Active control of flow around NACA 0015 airfoil by using DBD plasma actuator, *EPJ Web Conf*, 45 (2013) 01008, https://doi.org/10.1051/epjconf/20134501008.

16 Spalart P R & Allmaras S R, A one-equation turbulence model for aerodynamic flows, *AIAA Paper*, (1992) 439 , https://doi.org/10.2514/6.1992-439.

17 ANSYS Inc, *ANSYS Fluent Theory Guide*, Canonsburg (PA), ANSYS, 2023.

18 Enloe C L, McLaughlin T E, Van Dyken R D & Kachner K D, Plasma structure in the aerodynamic plasma actuator, *AIAA J*, 42 (3) (2004) 595, https://doi.org/10.2514/1.9104.

19 Benard N & Moreau E, *Exp Fluids*, 55 (11) (2014) 1846.

20 Suzen Y B, Huang P G & Jacob J D & Ashpis D E, Numerical simulations of plasma based flow control applications *AIAA Paper*, (2005) 4633, https://doi.org/10.2514/6.2005-4633.

21 Li X, Xu J & Zhang Y, *Aerosp Sci Technol*, 118 (2021) 107030.

22 West T K & Hosder S, *Int J Flow Control*, 5 (1) (2013), DOI: 10.2514/6.2012-3053.

23 Tang A, Li N, Price B, Mamishev A, Aliseda A & Novosselov I, *J Phys D Appl Phys*, 56 (35) (2023) 355201.